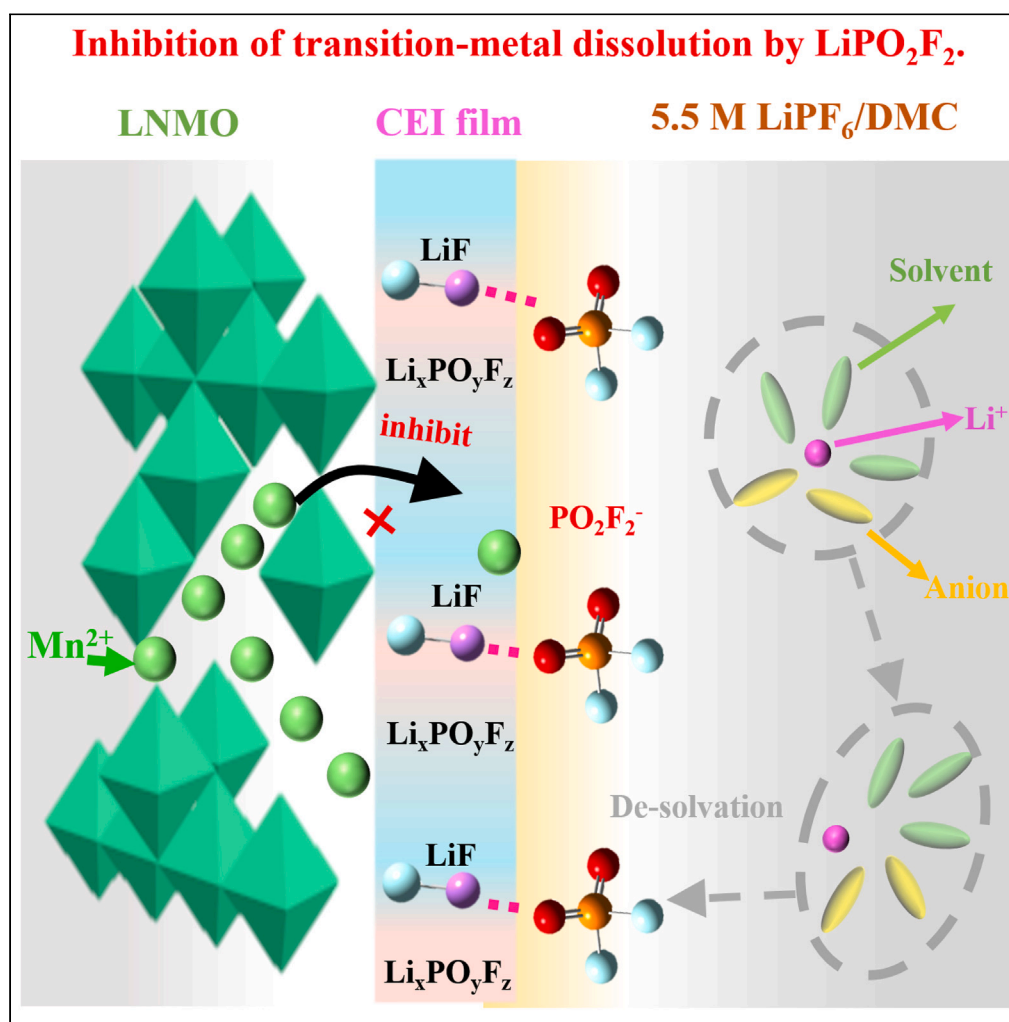## Article

Inhibition of transition-metal dissolution with an inert soluble product interface constructed by high-concentration electrolyte

Inhibition of transition-metal dissolution by $LiPO_2F_2$.

Shumin Wu,
Chunlei Li,
Jingjing Zhang, ...,
Jinlong Sun,
Xiaoling Cui,
Shiyou Li

lishiyoulw@163.com

Highlights

An anion-derived CEI film enriched in LiF and $LiPO_2F_2$ soluble product formed by HCEs

HCEs with DMC single solvent improve the cycling stability of LNMO‖Li cell at 55°C

An inert interface of $LiPO_2F_2$ soluble products can effectively inhibit HF corrosion

Article

Inhibition of transition-metal dissolution with an inert soluble product interface constructed by high-concentration electrolyte

Shumin Wu,[1,2] Chunlei Li,[1,2,3] Jingjing Zhang,[1,2] Peng Wang,[1,2] Dongni Zhao,[1,2,3] Yin Quan,[1,2] Jinlong Sun,[1,2] Xiaoling Cui,[1,2,3] and Shiyou Li[1,2,3,4,*]

SUMMARY

The formation of a compact and stable cathode electrolyte interphase (CEI) film is a promising way to improve the high voltage resistance of lithium-ion batteries (LIBs). However, challenges arise due to the corrosion of hydrogen fluoride (HF) and the dissolution of transition metal ions (TMs) in harsh conditions. To address this issue, researchers have constructed an anion-derived CEI film enriched with LiF and $LiPO_2F_2$ soluble product on the surface of $LiNi_{0.5}Mn_{1.5}O_4$ (LNMO) cathode in highly concentrated electrolytes (HCEs). The strong binding of LiF and $LiPO_2F_2$ generated an inert $LiPO_2F_2$ soluble product interface, which inhibited HF corrosion and maintained the spinel structure of LNMO, contributing to a capacity retention of 92% after 200 cycles at 55°C in the resulting cell with a soluble $LiPO_2F_2$-containing CEI film. This new approach sheds light on improving the electrode/electrolyte interface for high-energy LIBs.

INTRODUCTION

On the premise of ensuring safety performance, improving the energy density of lithium-ion batteries (LIBs) to more than 350Wh kg^{-1} has been the goal of research and development. The optimization of cathode materials is the key to achieve high energy density.[1-3] Among various cathode materials, the $LiNi_{0.5}Mn_{1.5}O_4$ (LNMO) spinel as a Co-free cathode has the merits of higher energy density (a high operating voltage of 4.7 V [vs. Li^+/Li] and a large specific capacity of 146.7 mAh g^{-1}), low cost, and being hypotoxic.[4-7] Unfortunately, some undesirable properties limit the practical application of LNMO, including side reactions between cathode and electrolyte, the dissolution of the transition metal ions (TMs), and subsequent deposit onto the anode during the cycles, especially at elevated temperatures and high voltage.[8-10] This is because hydrogen fluoride (HF) produced from the electrolyte may catalyze Mn (III) to form Mn^{4+} and Mn^{2+} ions. Insoluble Mn^{4+} ions may be deposited on the cathode surface, increasing the interface impedance of the cathode electrolyte interphase (CEI) film, while Mn^{2+} ions dissolve into the electrolyte and participate in the side reaction occurring at the anode.[11,12] Therefore, it is extremely necessary to build an effective CEI film to inhibit the corrosion of HF to the cathode and the side reaction induced by the TMs decomposition at the cathode interface.

In the past decades, many strategies have been implemented to strive for a stable and conductive CEI film to reduce the performance degradation of LNMO in three aspects: cathode material structure design, electrolyte formulation optimization, and interface film properties improvement.[13-15] A variety of "sacrificial" additives, such as lithium difluorophosphate ($LiPO_2F_2$), have been adopted to optimize electrolyte formulation.[16] On the one hand, they can form a passivation CEI film containing P-O species inhibiting the HF attack. On the other hand, they also help to increase the oxidation potential of the electrolyte at high voltage. And most studies have shown that $LiPO_2F_2$ would be preferentially oxidized at high voltage and form an inorganics-rich CEI with the advantages of low charge transfer resistance and suppressing the continuous electrolyte decomposition.[17,18] In addition, the development of highly concentrated electrolytes (HCEs)[19,20] have also been employed for high-voltage electrolytes. Considerable works indicated that the anions are predominantly oxidized to form an anion-derived CEI film on the cathode surface by increasing lithium salt concentration. In comparison with the solvent-derived CEI, the anion-derived CEI exhibits not only higher stability but also lower interfacial resistance for being rich in LiF, which is beneficial for inhibiting the dissolution of TMs at high voltage.[21]

[1]School of Petrochemical Technology, Lanzhou University of Technology, Lanzhou 730050, P.R. China

[2]Key Laboratory of Low Carbon Energy and Chemical Engineering of Gansu Province, Lanzhou 730050, P.R. China
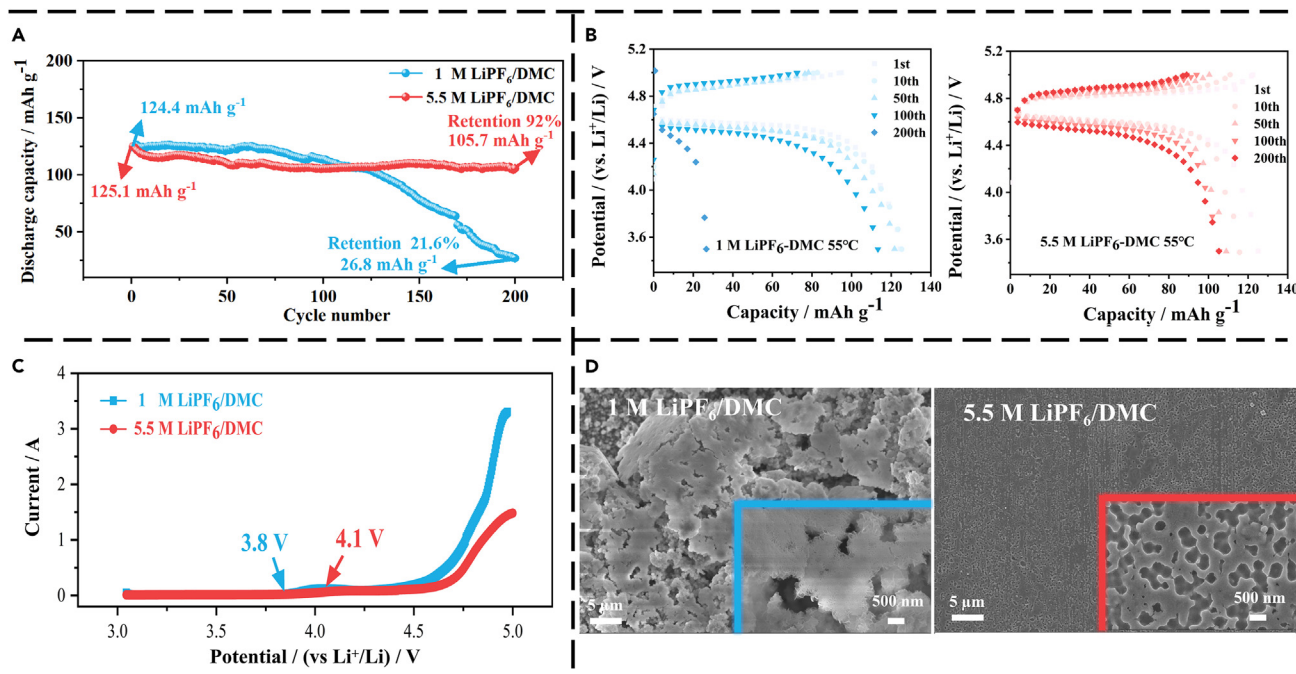
[3]Gansu Engineering Laboratory of Electrolyte Material for Lithium-ion Battery, Baiyin 730050, P. R. China

[4]Lead contact

*Correspondence: lishiyoulw@163.com

https://doi.org/10.1016/j.isci.2023.107052

Figure 1. Electrochemical performance of LNMO‖Li half cells using 1 M LiPF$_6$/DMC and 5.5 M LiPF$_6$/DMC

(A) Cyclic performance of the first 200 cycles from within 3.5–5.0 V at 2 C, 55°C.

(B) Charge-discharge profiles of selected cycles from (A).

(C) LSV profiles within 3.5–5.0 V at 2 C, 55 °C.

(D) SEM images of Li‖Al half cells preserved under 5.5 V after three days.

However, the previous explanation of the mechanism of electrolyte formulation optimization to the CEI film mainly focused on the analysis of the influence of insoluble products deposited on the electrode surface on the electrode performance. Recently, the influence of the soluble products of the electrolyte on battery performance is gradually attracting researchers' attention. For example, Hehschel et al.[22] found that there were some soluble products in the electrolyte derived from the side reactions. Biswal et al.[23] also studied how to regulate the favorable components of electrolyte electrode interface (EEI) film to form insoluble products and the unfavorable components to form soluble products to promote the dissolution and removal of undesirable components. What's more, the previous studies in our groups have shown that different from conventional concentration electrolytes (CCEs), due to more PF$_6^-$ anions participating in oxidation decomposition in HCEs, an anion-derived CEI film consisting of LiF, Li$_x$PO$_y$F$_z$, and Li$_3$PO$_4$ was formed, where Li$_x$PO$_y$F$_z$ was formed by the oxidation of PF$_6^-$, and Li$_3$PO$_4$ were generated by soluble PO$_2$F$_2^-$ from the hydrolysis of LiPF$_6$.[24] The hydrolysis reaction of PF$_6^-$ in HCEs produces large soluble products of LiPO$_2$F$_2$ enriching on the electrode surface, which was found to be able to prohibit the successive decomposition of electrolytes and improve the conductivity.[25,26] However, the role of soluble products for high-voltage battery systems and their working mechanisms on the CEI film have not been studied so far. In addition, similar to our work, a Li$_x$PO$_y$F$_z$-rich CEI film was proved to provide effective protection by isolating the contact between the residue of solvent molecules and the highly active cathode surface.[27] Increasing the product concentration of Li$_x$PO$_y$F$_z$ in CEI film helps to effectively enhance the high voltage resistance of the electrolyte and thus promotes the performance of LIBs.[28]

Herein, to understand the role of soluble products in improving the Li$^+$ diffusion dynamics and inhibiting HF attacks, we propose an inert LiPO$_2$F$_2$ soluble products interface derived from HCEs. Through theoretical calculation and experimental analyses, it is found that a Li$_x$PO$_y$F$_z$ and LiPO$_2$F$_2$ soluble products-derived CEI film in HCEs is formed on the LNMO cathode surface. It is beneficial to improve the Li$^+$ ions diffusion dynamics and inhibit the solution of TMs.[29] Importantly, the strong binding energy and the barrier effect of LiPO$_2$F$_2$ soluble products are put forward to explain the improved properties of high-voltage LNMO cells and inhibit HF corrosion with HCEs at elevated temperatures. This new point of view sheds a different light on optimizing high-voltage electrolytes by constructing soluble products-derived interface.
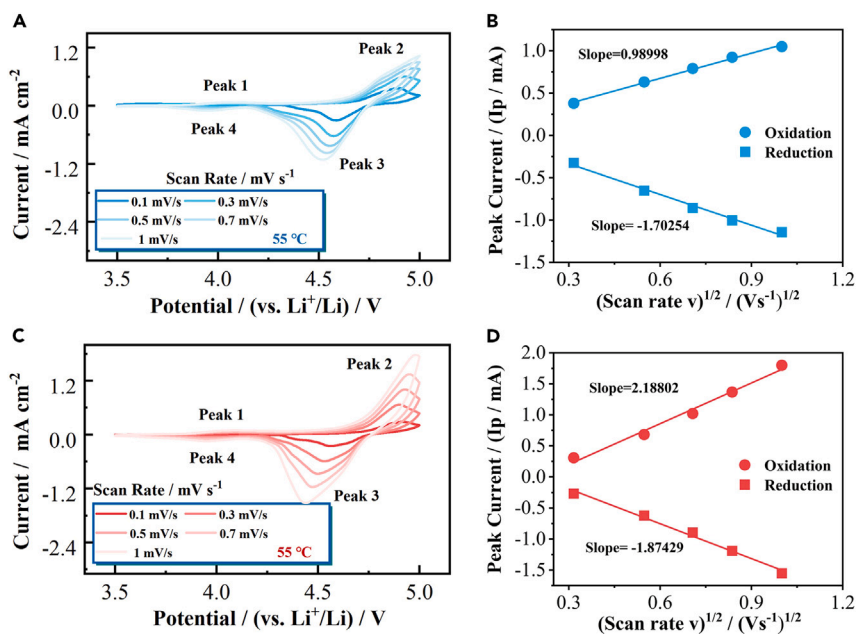
Figure 2. CV curves of LNMO||Li half cells with two kinds of electrolyte at different scan rates from 0.1 to 1.0 mV s^{-1} at 55°C and corresponding Randles-Sevcik curves

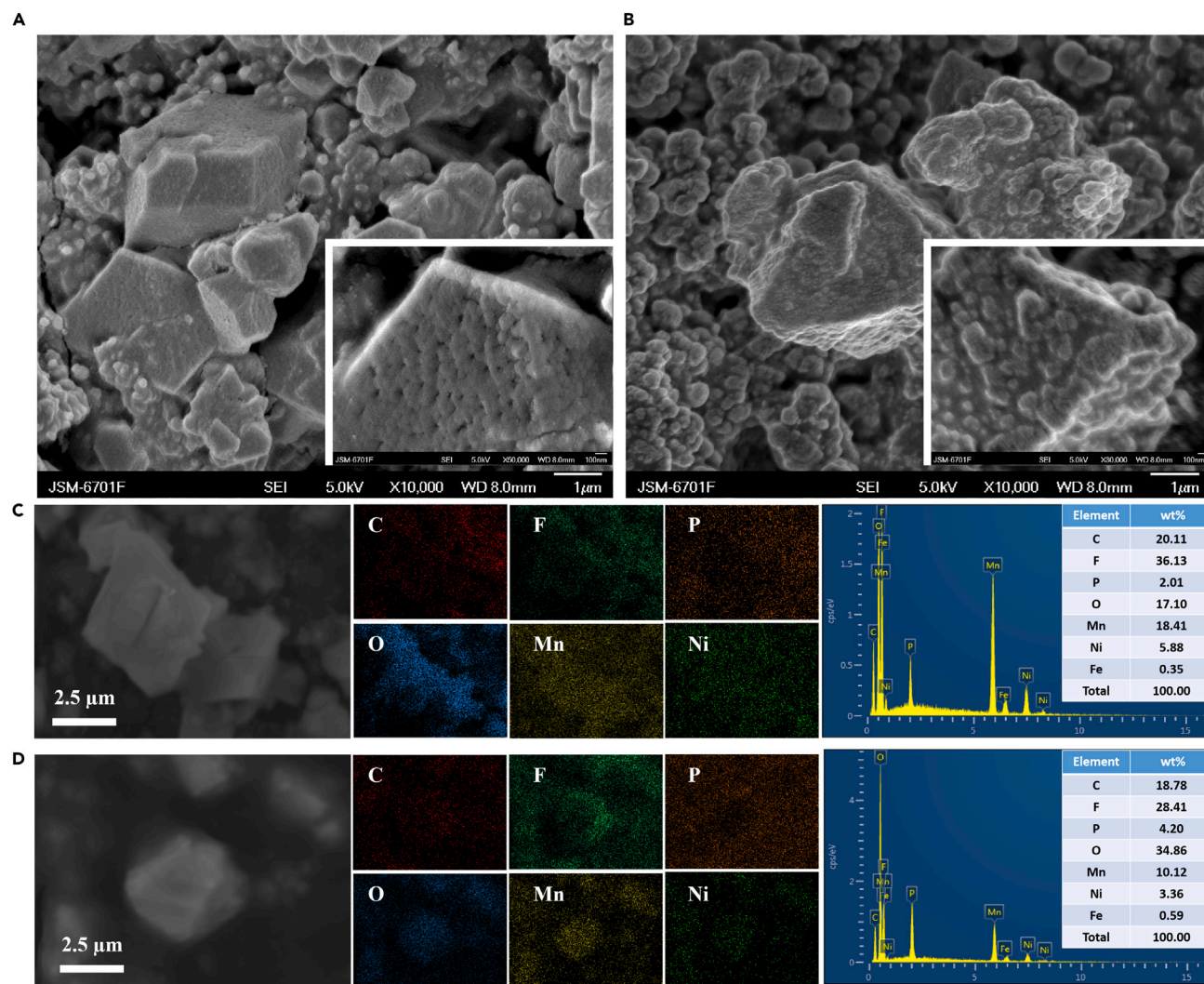(A and B) 1 M LiPF$_6$/DMC and (C and D) 5.5 M LiPF$_6$/DMC.

RESULTS

Electrochemical performance analysis

A comparison of cyclic stability of LNMO in CCEs and HCEs is presented in Figure 1, which demonstrates that 5.5 M LiPF$_6$/(dimethyl carbonate) DMC can enhance the cyclic stability of LNMO||Li half cells when increasing the concentration of lithium salt. The discharge capacity of LNMO cycled with different concentration electrolytes presents a slow decay in the initial 120 cycles (Figure 1A), which can be ascribed to the increased interface resistance originating from the successive decomposition of the electrolyte. After 120 cycles, the discharge capacity of 1 M LiPF$_6$/DMC drops dramatically, and capacity retention of only 21.6% is achieved at the 200th cycle. This is because HF generated by the decomposition of electrolyte will attack the cathode surface and accelerate the dissolution of TMs, which damages the interphase seriously.[30] Whereas outstanding cyclic stability was performed in 5.5 M LiPF$_6$/DMC with a capacity retention of 92%. It means that the interface film formed by HCEs effectively inhibits HF corrosion.

Linear sweep voltammetry (LSV) measurement was further conducted to evaluate the intrinsic oxidation and reduction stability at different concentrations of LiPF$_6$ in the DMC of the Li||Al half cells (Figure 1C). Compared with the low oxidation voltage of 1 M LiPF$_6$/DMC (~3.8 V vs. Li$^+$/Li), 5.5 M LiPF$_6$/DMC has a higher oxidation voltage (~4.1 V), indicating that the HCEs have a greater high voltage resistance and therefore have a better cycling performance. In addition, the scanning electron microscope (SEM) images of Li||Al half cells preserved under 5.5 V after three days show that the aluminum foil in 5.5 M LiPF$_6$/DMC keeps intact, while large uneven lithium deposits on aluminum foil and make corrosion in 1 M LiPF$_6$/DMC (Figure 1D), perhaps for reason that improving the concentration of LiPF$_6$ is responsible for inhibiting the corrosion of aluminum foil by decomposing and producing HF with trace water and then generating an AlF$_3$ layer with Al.[31] The superior oxidation resistance and corrosion resistance show that the HCEs system can resist the attack of HF.

It concludes that HCEs can alleviate the corrosion of HF by increasing the concentration of LiPF$_6$ and keeping more intact aluminum foil, improving the cyclic stability of LNMO at high temperatures and high potential. This is consistent with previous research results; that is, HCEs have achieved good effects in broadening the electrochemical stability window of electrolytes and inhibiting the corrosion of HF.

Figure 3. SEM and EDS images and the corresponding EDS analysis of surface element distribution of LNMO electrodes of LNMO||Li half cells after 200 cycles at 2C, 55°C with different concentrations of electrolytes

(A and C) 1 M LiPF$_6$/DMC and (B and D) 5.5 M LiPF$_6$/DMC.

Diffusion dynamics behavior analysis

Considering that the introduction of a high concentration of lithium salt will cause large viscosity of electrolytes, which may affect the transmission rate of Li$^+$ ions, it is necessary to compare the diffusion dynamics of Li$^+$ ions in electrolytes with different concentrations. In Figure 2, we show the cyclic voltammetry (CV) response of LNMO||Li half cells with 1 M LiPF$_6$/DMC (Figure 2A) or 5.5 M LiPF$_6$/DMC (Figure 2C) for scan rates ranging from 0.1 to 1.0 mV s^{-1} at 55°C. The voltage scan from 3.5 to 5.0 V results in a symmetric current response centered at around a voltage of 4.7 V. Compared with 1 M LiPF$_6$/DMC, the CV response for the 5.5 M LiPF$_6$/DMC reveals a much higher maximum current value for the corresponding scan rates (Peak 2 on Figures 2A and 2C). In the scanning direction, the current value rises rapidly toward the current maxima and has no obvious falling off for 1 M LiPF$_6$/DMC at high scan rates but falls off slowly for 5.5 M LiPF$_6$/DMC, due to the facts that 1) DMC has fast solvation kinetics,[32] but high lithium salt concentration inhibits the solvent migration rate to a certain extent and/or 2) 5.5 M LiPF$_6$/DMC reduced area of accessible unreacted electrode surface by preferentially oxidative decomposition at lower voltages.

The Randles-Sevcik equation depicts the relationship of the cathodic and anodic current peaks (Ip) versus the square root of scan rates (v$^{0.5}$) for 1 M LiPF$_6$/DMC and 5.5 M LiPF$_6$/DMC, whose slope can be used to
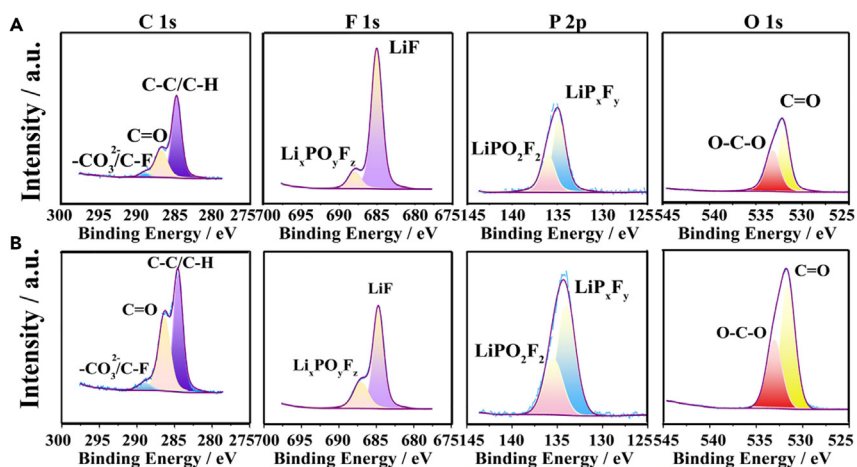
Figure 4. The results of LNMO electrodes from LNMO||Li half cells after 200 cycles at 2 C, 55°C
(A) The XPS result of electrolyte of 1 M LiPF$_6$/DMC of C 1s, F 1s, P2p, and O 1s.
(B) The XPS result of electrolyte of concentration of 5.5 M LiPF$_6$/DMC of C 1s, F 1s, P2p, and O 1s.

compare the apparent diffusivity of Li$^+$ ions qualitatively (Figures 2B and 2D).[33] As shown in Figure 2, the slopes of 5.5 M LiPF$_6$/DMC (2.18802 and −1.70254) are higher than those in 1 M LiPF$_6$/DMC (2.18802 and −1.70254) for the oxidation and reduction process, respectively. The results show that HCEs have faster Li$^+$ ions diffusion dynamics, which may be attributed to better surface films with higher lithium ions conductivity, a peculiar electrical double layer, or better Li$^+$ ions de-solvation kinetics compared to 1 M LiPF$_6$/DMC. The current research focus is on how HCEs improve the composition and structure of the CEI film by special solvated structure, which is conducive to improving the comprehensive performance of the battery. Accordingly, we may focus on the composition and properties of CEI film by the decomposition products of HCEs involved in the charge-discharge process systematically.

Surface analysis

In order to investigate the impact of HCEs electrolyte on preserving the stability of LNMO electrode structure and the uniformity of CEI film under high voltage and elevated temperatures, we employed SEM and energy dispersive spectrometer (EDS) measurements to observe the surface morphology and element mapping of cycled electrodes. The surface morphologies of LNMO electrodes examined after 200 cycles at 55°C are shown in Figure 3. An incomplete CEI film with a large number of cracks can be observed on the cycled-electrode surfaces in 1 M LiPF$_6$/DMC electrolyte (Figure 3A). It should be associated with the corrosion caused by poor mechanical properties of CEI film formed in 1 M LiPF$_6$/DMC, failing to protect from HF attack during the long cycle at 55°C. Compared with 1 M LiPF$_6$/DMC, the surface of HCEs shows a complete CEI film with a large number of deposited particles, which well maintains the spinel structure of LNMO, inhibiting the corrosion of HF effectively (Figure 3B). Besides, it can be seen from EDS images that the Mn and Ni elements content of 1 M LiPF$_6$/DMC (Figure 3C) are significantly higher than that of 5.5 M LiPF$_6$/DMC (Figure 3D), suggesting that a more uniform CEI film was formed by HCEs. Despite this, there are only a few studies on how HCEs can alleviate the severe side effects resulting from HF corrosion. Therefore, to verify the above conjecture, we conducted an analysis of the reductive decomposition products of electrolytes with different concentrations, along with a qualitative examination of TM dissolution across different systems.

CEI film components analysis

The X-ray photoelectron spectroscopy (XPS) spectra of LNMO anodes after 200 cycles are depicted to study the component information of CEI film in Figure 4. The XPS data are corrected by C 1s (284.8 eV) of contaminated carbon and fitted by Avantage software. There are three distinct peaks in the C 1s spectrum of LNMO anode, including C-C/C-H (~284.8 eV), C=O (~288.4 eV), and − CO_3^{2-}/C-F (~291 eV). The presence of the C-C bond (originated from carbon black), C=O bond (classified to O-CO$_2^-$ group), and − CO_3^{2-}/C-F bond (derived from the conductive carbon additive and the carbon binder) indicates the formation of alkyl lithium carbonate (ROCO$_2$Li), ROLi, and lithium carbonate (Li$_2$CO$_3$) species on the cathode surface, which originated from the decomposition of LiPF$_6$-salt or DMC solvent. LiF (~686 eV) and Li$_x$PO$_y$F$_z$
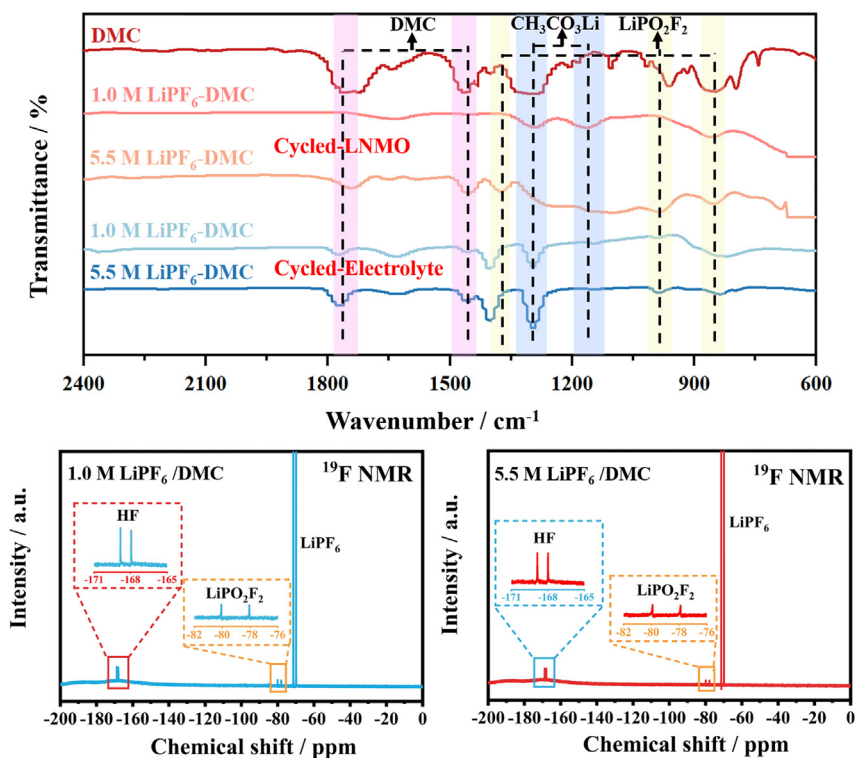
Figure 5. The testing results of different electrolytes from LNMO‖Li half cells after 200 cycles at 2 C, 55°C
(A) The FTIR spectra of the cycled-LNMO surface and cycled-electrolyte with 1 M LiPF$_6$/DMC and 5.5 M LiPF$_6$/DMC,respectively.
(B and C) ^{19}F NMR spectra with different electrolytes from cycled-electrolyte of 1 M LiPF$_6$/DMC and 5.5 M LiPF6/DMC, respectively.

($\sim$688.4 eV) are the two characteristic peaks in the F 1s spectrum of the LNMO cathode. Besides, two characteristic peaks of LiP$_x$F$_y$ ($\sim$133.2 eV) and LiPO$_2$F$_2$ ($\sim$135.4 eV) are found in the P 2p spectrum. The results show that the peak intensity of Li$_x$PO$_y$F$_z$ enhances and a CEI film mainly composed of LiF and LiPO$_2$F$_2$ is formed with the increasing concentration of LiPF$_6$.[34] There are slight shifts in the peak positions corresponding to P 2p of LiPO$_2$F$_2$ species, which can be mainly attributed to the F-O interaction that affects the intermolecular attraction and binding energy between two ions. In addition, LiPO$_2$F$_2$ is reported to be able to form a low-charge-transfer-resistance CEI film and improves the transport rate of Li$^+$ in HCEs, which is consistent with the above CV conclusions.[17]

The Fourier transform infrared (FTIR) spectrometer was also employed to further analyze the decomposition products of electrolytes on the LNMO surface. Cycled-LNMO reflects the decomposition products of the LNMO electrode surface formed in the different electrolytes after 200 cycles and washing with DMC solvent, while cycled electrolyte responds to the flushing fluid of Cycled-LNMO with DMC solvent, which reflects some soluble products dissolved in the electrolyte. As shown in Figure 5A, the absorption peaks at around 1743 cm^{-1} (υ: C=O) and 1456 cm^{-1} (υ_{as}: CO$_3^{2-}$) are the characteristic peaks of DMC (the first curve).[35] After cycling, the peaks of the C=O and CO$_3^{2-}$ bonds on the LNMO surface with 1 M LiPF$_6$/DMC disappear and the new absorption peaks at around 1295 cm^{-1} (υ_s: C=O) and 1160 cm^{-1} (υ_{as}: C-O) appear (the second curve). The results show the formation of CH$_3$CO$_3$Li-containing CEI films in 1 M LiPF$_6$/DMC and also indicate the formation of solvent-derived CEI films in CCEs. The three characteristic peaks at around 1397 cm^{-1} (υ_{as}: O=P-O), 1104 cm^{-1} (υ_s: O=P-O), and 849 cm^{-1} (υ: P-F) appear on the Cycled-LNMO surface with 5.5 M LiPF$_6$/DMC (the third curve).[36,37] The higher viscosity of HCEs leads to the deposition of an increased volume of LiPO$_2$F$_2$ decomposition products on the surface of CEI film. LiPO$_2$F$_2$ has been previously utilized as an additive for enhancing the rate performance of LIBs, indicating its solubility and existence as soluble products in HCEs. Besides, by detecting the cycled electrolyte, we confirmed the existence of LiPO$_2$F$_2$ in various electrolytes where it predominantly exists as soluble products. We further supplemented the nuclear magnetic resonance (NMR) test to evaluate the soluble

Table 1. Content of transition metals and P elements on the separator surface after 200 cycles determined by ICP-OES

Separator	Element (ppm) %	
	P	Mn
with 1 M LiPF$_6$/DMC	2.36	5.11
with 5.5 M LiPF$_6$/DMC	7.99	1.03

species information in cycled electrolyte from electrolytes with different concentrations assembled in the LNMO‖ Li half cells. As shown in Figures 5B and 5C, the ^{19}F NMR spectra of electrolytes with different concentrations have two small peaks of HF and LiPO$_2$F$_2$, which correspond to peaks at approximately 168 ppm (HF) and 80 ppm (LiPO$_2$F$_2$).[38] According to those findings, HCEs tend to generate a large amount of LiPO$_2$F$_2$ soluble products, whereby a portion of such products accumulates onto the surface of LNMO electrodes, which is consistent with the result of XPS.

It is currently unclear whether these soluble products exhibit similar or distinct effects to additives in terms of inhibiting HF corrosion. Thus, we qualitatively analyzed the dissolution of TMs in different systems by inductively coupled plasma optical emission spectrometer (ICP-OES). High temperature and voltage cause larger TMs from the cathode to migrate through the separator and deposit on the anode, leading to secondary effects and capacity decay during long cycles.[39,40] The TMs contents detected on the separator surface are more indicative of the dissolved status of TMs. Hence, to clarify the inhibition effect of CEI film formed with different concentration electrolytes on the TMs dissolution, the TMs contents of 200 cycled separators were measured by ICP-OES (Table 1). The results show that the Mn content detected in 1 M LiPF$_6$/DMC is almost five times higher than that in 5.5 M LiPF$_6$/DMC. Combined with FTIR and XPS data, this behavior can be explained by the rationale that the dissolution of TMs is inhibited by HCEs. The significance of LiPO$_2$F$_2$ is evident, which has been demonstrated to possess the ability to halt HF corrosion and prohibit the successive decomposition of electrolytes.[41] Therefore, the theoretical calculation will be employed to explain the working mechanism of these LiPO$_2$F$_2$ soluble products in inhibiting the attack of HF.

Mechanism

Density functional theory (DFT) has been used to investigate the effect of LiPO$_2$F$_2$ on the CEI film interface. The geometry optimization of LiF-PF$_6^-$ and LiF-PO$_2$F$_2^-$ was carried out with the basis set of B3LYP/6–311 + G (2 days, p) and shown in Figure 6. Unlike the oxidation analysis of mixed solvent molecules, we analyzed the interaction between LiF and PF$_6^-$ or PO$_2$F$_2^-$. As a strong interionic interaction between Li$^+$ and F$^-$, a LiF-rich CEI film forms at the electrode interface in HCEs, which can inhibit solvent co-intercalation. What's more, it was reported that a LiF-rich interface may affect the orientation of anions in the electrolyte.[42] Especially with the increase of lithium salt concentration in the electrolyte, the probability of ion interaction increases in the LiF-rich interface. It was shown in Figure 6A that PO$_2$F$_2^-$ has higher binding energy than PF$_6^-$ with LiF, which means that more PO$_2$F$_2^-$ anions are easily enriched at the LiF interface, while PF$_6^-$ anions are excluded at a distance from the hetero-interface. Since LiPO$_2$F$_2$ can be dissolved in the electrolyte as soluble products, the concentration of PO$_2$F$_2^-$ anions in the electrolyte will increase with the increase of the charging process, resulting in a concentration gradient between the near surface of the electrode and the bulk electrolyte. Under the influence of the strong electric field effect of LiF, a CEI film enriched with PO$_2$F$_2^-$ anions is formed at the fluorine-containing interface. Hence, we believe that a LiPO$_2$F$_2$ soluble product interface was formed on the CEI film surface in HCEs.

And then, the reactivity of the LiPO$_2$F$_2$ (main components of CEI film in HCEs) and CH$_3$CO$_3$Li (main components of CEI film in CCEs) with an HF molecule was calculated. In Figure 6B, the reactions with HF via the O-Li bond and O-CH$_3$ bond cleavages are considered, respectively. It has been shown that the reactions between LiPO$_2$F$_2$ species and HF are not permitted ($\Delta G = 152.05$ kcal mol^{-1}). Similar to LiPO$_2$F$_2$, the Gibbs free energy between CH$_3$CO$_3$Li and LiF is positive for the O-Li bond (132.34 kcal mol^{-1}) cleavages. It is worth noting that CH$_3$CO$_3$Li and HF can occur in a favorable reaction by the O-CH$_3$ bond ($\Delta G = -459.27$ kcal mol^{-1}) cleavage, and the reaction products are FCO$_3$Li and CH$_4$. This is in good harmony with experimental results that the CH$_3$CO$_3$Li is unable to resist the attack of HF, resulting in the dissolution of a large number of TMs, but the inert LiPO$_2$F$_2$ soluble products interface can form a barrier to prevent HF's corrosion. In addition, considering the solubility feature of LiPO$_2$F$_2$, it was
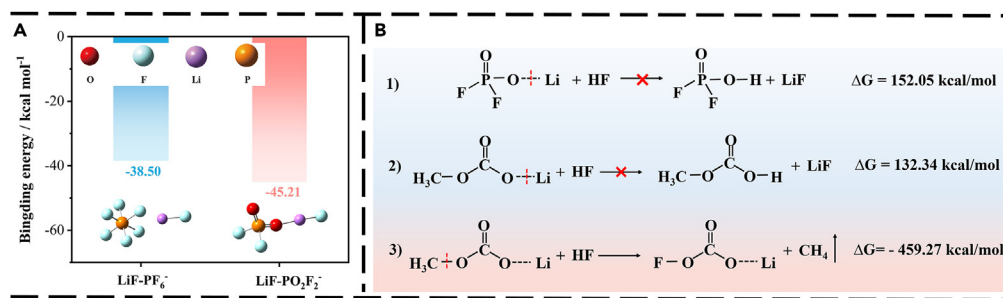
Figure 6. The calculation results of different solvation molecule structures
(A) The binding energies of different solvation molecule structures for LiF-PF$_6$ and LiF-PO$_2$F$_2^-$.
(B) Gibbs free energy (ΔG) of LiPO$_2$F$_2$ and CH$_3$CO$_3$Li with an HF molecule.

supposed that the inhibition effect on HF corrosion will increase with the increase of PO$_2$F$_2^-$ anion layer on the electrode surface.

The corresponding schematic is shown in Figure 7. In the CCEs (Figure 7A), solvent molecules mainly participate in the formation of a solvated sheath and generate a large number of LiF and CH$_3$CO$_3$Li at the electrode interface, resulting in a solvent-derived CEI film. However, CH$_3$CO$_3$Li can react with HF easily, which leads to the dissolution of the CEI film. This makes HF to be in direct contact with the LNMO electrode, causing the dissolution of TMs and the structural collapse of the LNMO cathode.

In the HCEs (Figure 7B), more anions from lithium salt participate in the formation of a solvation sheath, which can preferentially undergo oxidation, resulting in an anion-derived CEI film. An anion-derived CEI film mainly composed of LiF and Li$_x$PO$_y$F$_z$ was formed on the LNMO cathode surface. More importantly, because of the strong electric field of LiF, a large amount of PO$_2$F$_2^-$ anions attracted and enriched on the CEI surface, and an interface surrounded by LiPO$_2$F$_2$ soluble products is formed. This LiPO$_2$F$_2$ soluble product will construct an inert barrier to inhibit the attack of HF on the LNMO electrode and hinder the dissolution of TMs. Thus, the oxidation stability of HCEs is significantly improved and exhibits excellent cycle performance and capacity retention under stringent conditions.

DISCUSSION

Our study systematically examined how HCEs can enhance the capacity and cyclic performance of the highly promising LNMO cathode under high-temperature (55°C) and high-voltage (5.0 V) conditions. The LNMO||Li half cell with HCEs delivers a specific capacity of 127.5 mAh g^{-1} at 2C, which is much higher than that with 1 M LiPF$_6$/DMC (80.5 mAh g^{-1}). The action mechanism of HCEs in the high-voltage system is analyzed in detail through characterization and theoretical calculation. Different from the traditional point of view, we propose that an anion-derived CEI film formed on the LNMO cathode surface is mainly composed of LiF and LiPO$_2$F$_2$ soluble products, which can not only improve the Li$^+$ diffusion dynamics but also enhance the cycle stability. The strong binding energy of LiF and LiPO$_2$F$_2$ results in a protective barrier effect that prevents HF from corroding the LNMO surface, consequently impeding the dissolution of TMs and mitigating battery performance degradation. Thereupon, regulating anion-derived CEI film by forming a LiPO$_2$F$_2$ soluble product inert interface is a promising method to improve the high energy density and cyclic stability of LNMO batteries.

Limitations of the study

The study found that high-concentrated electrolytes regulate anion-derived CEI film by forming a LiPO$_2$F$_2$ soluble product inert interface, which effectively inhibits HF attack on LNMO electrode and the leaching of TMs. Due to the limitations of current characterization tools, how the formation, presence, and solubility of soluble products affect battery performance has not been thoroughly studied.

STAR★METHODS

Detailed methods are provided in the online version of this paper and include the following:

- KEY RESOURCES TABLE
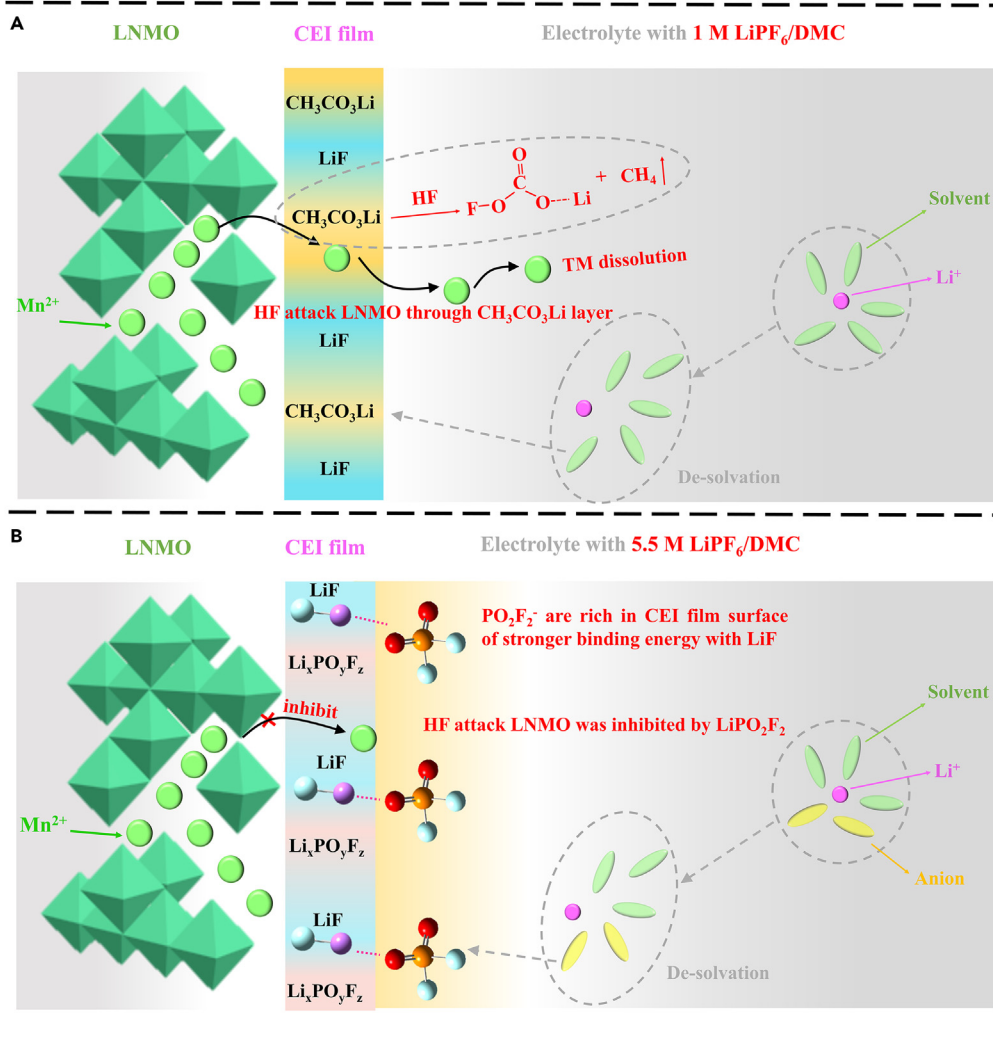
Figure 7. The mechanism schematic of HF attack the CEI film on LNMO cathode
(A) With electrolyte of concentration of 1 M $LiPF_6$/DMC.
(B) With electrolyte of concentration of 5.5 M $LiPF_6$/DMC.

- **RESOURCE AVAILABILITY**
  - Lead contact
  - Materials availability
  - Data and code availability
- **METHOD DETAILS**
  - Preparation of electrolytes and electrodes
  - Battery assembly and electrochemical measurements
  - Characterization
  - Theoretical calculations

AUTHOR CONTRIBUTIONS

SMW performed experiments and wrote the original draft of the manuscript. SYL and CLL led and supported the funding acquisition for the project. JJZ and PW modeled the dataset. YQ, DNZ, and XLC contributed to the review and editing of the manuscript. All authors approved the final version of the manuscript.

DECLARATION OF INTERESTS

The authors declare no competing interests.

REFERENCES

1. Yu, J., Hu, Y., Ma, X., Zou, X., Qi, H., Zhou, Y., and Yan, F. (2022). A highly conductive and stable hybrid solid electrolyte for high voltage lithium metal batteries. J. Mater. Chem. *10*, 12842–12855.

2. Chen, M., Wang, W., Shi, Z., Liu, Z., and Shen, C. (2022). Revealing the cathode electrolyte interphase on Li- and Mn- rich materials by in-situ electrochemical atomic force microscopy. Appl. Surf. Sci. *600*, 154119.

3. Wang, P., Yan, D., Wang, C., Ding, H., Dong, H., Wang, J., Wu, S., Cui, X., Li, C., Zhao, D., and Li, S. (2022). Study of formation and evolution of solid electrolyte interface by in-situ electrochemical impedance spectroscopy. Appl. Surf. Sci. *596*, 153572.

4. Chu, C.T., Mondal, A., Kosova, N.V., and Lin, J.Y. (2020). Improved high-temperature cyclability of AlF_3 modified spinel $LiNi_{0.5}Mn_{1.5}O_4$ cathode for lithium-ion batteries. Appl. Surf. Sci. *530*, 147169.

5. Ma, J., Hu, P., Cui, G., and Chen, L. (2016). Surface and interface issues in spinel $LiNi_{0.5}Mn_{1.5}O_4$: insights into a potential cathode material for high energy density Lithium-ion batteries. Chem. Mater. *28*, 3578–3606.

6. Lahiru Sandaruwan, R.D., Cong, L., Ma, L., Ma, S., and Wang, H. (2021). Tackling the interfacial issues of spinel $LiNi_{0.5}Mn_{1.5}O_4$ by room-temperature spontaneous dediazonation reaction. ACS Appl. Mater. Interfaces *13*, 1313264–1313272.

7. Lee, T.J., Soon, J., Chae, S., Ryu, J.H., and Oh, S.M. (2019). Bifunctional electrolyte additive for high-voltage $LiNi_{0.5}Mn_{1.5}O_4$ positive electrodes. ACS Appl. Mater. Interfaces *11*, 11306–11316.

8. Wang, K., Xing, L., Zhu, Y., Zheng, X., Cai, D., and Li, W. (2017). A comparative study of Si-containing electrolyte additives for lithium ion battery: which one is better and why is it better. J. Power Sources *342*, 677–684.

9. Zhan, C., Lu, J., Jeremy Kropf, A., Wu, T., Jansen, A.N., Sun, Y.K., Qiu, X., and Amine, K. (2013). Mn (II) deposition on anodes and its effects on capacity fade in spinel lithium manganate-carbon systems. Nat. Commun. *4*, 2437.

10. Ma, L., Nie, M., Xia, J., and Dahn, J.R. (2016). A systematic study on the reactivity of different grades of charged $Li[Ni_xMn_yCo_2]O_2$ with electrolyte at elevated temperatures using accelerating rate calorimetry. J. Power Sources *327*, 145–150.

11. Ko, D.S., Park, J.H., Park, S., Ham, Y.N., Ahn, S.J., Park, J.H., Han, H.N., Lee, E., Jeon, W.S., and Jung, C. (2019). Microstructural visualization of compositional changes induced by transition metal dissolution in Ni-rich layered cathode materials by high-resolution particle analysis. Nano Energy *56*, 434–442.

12. Lee, Y.K. (2021). Effect of transition metal ions on solid electrolyte interphase layer on the graphite electrode in lithium-ion battery. J. Power Sources *484*, 229270.

13. Wang, J., Dong, H., Wang, P., Fu, X.L., Zhang, N.S., Zhao, D.N., Li, S.Y., and Cui, X.L. (2022). Adjusting the solvation structure with tris(trimethylsilyl)borate additive to improve the performance of LNCM half cells. J. Energy Chem. *67*, 55–64.

14. Luan, X., Qi, L., Zheng, Z., Gao, Y., Xue, Y., and Li, Y. (2023). Step by step induced growth of Zinc-metal interface on graphdiyne for aqueous Zinc-ion batteries. Angew. Chem. Int. Ed. Engl. *62*, e202215968.

15. Fang, Y., Liu, Y., Qi, L., Xue, Y., and Li, Y. (2022). 2D graphdiyne: an emerging carbon material. Chem. Soc. Rev. *51*, 2681–2709.

16. Shangguan, X., Xu, G., Cui, Z., Wang, Q., Du, X., Chen, K., Huang, S., Jia, G., Li, F., Wang, X., et al. (2019). Additive-assisted novel dual-salt electrolyte addresses wide temperature operation of lithium-metal batteries. Small *15*, 1900269.

17. Chen, J., Xing, L., Yang, X., Liu, X., Li, T., and Li, W. (2018). Outstanding electrochemical performance of high-voltage $LiNi_{1/3}Co_{1/3}Mn_{1/3}O_2$ cathode achieved by application of $LiPO_2F_2$ electrolyte additive. Electrochim. Acta *290*, 568–576.

18. Kuang, S., Hua, H., Lai, P., Li, J., Deng, X., Yang, Y., and Zhao, J. (2022). Anion-containing solvation structure reconfiguration enables wide-temperature electrolyte for high-energy-density lithium metal batteries. ACS Appl. Mater. Interfaces *14*, 19056–19066.

19. Qian, J., Henderson, W.A., Xu, W., Bhattacharya, P., Engelhard, M., Borodin, O., and Zhang, J.G. (2015). High rate and stable cycling of lithium metal anode. Nat. Commun. *6*, 6362.

20. Jie, Y., Liu, X., Lei, Z., Wang, S., Chen, Y., Huang, F., Cao, R., Zhang, G., and Jiao, S. (2020). Enabling high-voltage lithium metal batteries by manipulating solvation structure in ester electrolyte. Angew. Chem. Int. Ed. Engl. *59*, 3505–3510.

21. Liu, W., Li, J., Li, W., Xu, H., Zhang, C., and Qiu, X. (2020). Inhibition of transition metals dissolution in cobalt-free cathode with ultrathin robust interphase in concentrated electrolyte. Nat. Commun. *11*, 3629.

22. Henschel, J., Peschel, C., Günter, F., Reinhart, G., Winter, M., and Nowak, S. (2019). Reaction product analysis of the most active "inactive" material in lithium-ion batteries-the electrolyte. II: battery operation and additive impact. Chem. Mater. *31*, 9977–9983.

23. Biswal, P., Rodrigues, J., Kludze, A., Deng, Y., Zhao, Q., Yin, J., and Archer, L.A. (2022). A reaction-dissolution strategy for designing solid electrolyte interphases with stable energetics for lithium metal anodes. Cell Rep. Phys. Sci. *3*, 100948.

24. Cui, X., Zhang, J., Wang, J., Wang, P., Sun, J., Dong, H., Zhao, D., Li, C., Wen, S., and Li, S. (2021). Antioxidation mechanism of highly concentrated electrolytes at high voltage. ACS Appl. Mater. Interfaces *13*, 59580–59590.

25. Jiang, B., Li, J., Luo, B., Yan, Q., Li, H., Liu, L., Chu, L., Li, Y., Zhang, Q., and Li, M. (2021). $LiPO_2F_2$ electrolyte additive for high-performance Li-rich cathode material. J. Energy Chem. *60*, 564–571.

26. Zhao, W., Zheng, G., Lin, M., Zhao, W., Li, D., Guan, X., Ji, Y., Ortiz, G.F., and Yang, Y.

(2018). Toward a stable solid-electrolyte-interfaces on nickel-rich cathodes: LiPO$_2$F$_2$ salt-type additive and its working mechanism for LiNi$_{0.5}$Mn$_{0.25}$Co$_{0.25}$O$_2$ cathodes. J. Power Sources *380*, 149–157.

27. Chen, J., Liu, T., Gao, L., Qian, Y., Liu, Y., and Kong, X. (2021). Tuning the solution structure of electrolyte for optimal solid-electrolyte-interphase formation in high-voltage lithium metal batteries. J. Energy Chem. *60*, 178–185.

28. Wu, F., Dong, J., Chen, L., Bao, L., Li, N., Cao, D., Lu, Y., Xue, R., Liu, N., Wei, L., et al. (2021). High-voltage and high-safety nickel-rich layered cathode enabled by a self-reconstructive cathode/electrolyte interphase layer. Energy Storage Mater. *41*, 495–504.

29. Zhang, Q., Pan, J., Lu, P., Liu, Z., Verbrugge, M.W., Sheldon, B.W., Cheng, Y.T., Qi, Y., and Xiao, X. (2016). Synergetic effects of inorganic components in solid electrolyte interphase on high cycle efficiency of lithium-ion batteries. Nano Lett. *16*, 2011–2016.

30. Pieczonka, N.P.W., Liu, Z., Lu, P., Olson, K.L., Moote, J., Powell, B.R., and Kim, J.H. (2013). Understanding transition-metal dissolution behavior in LiNi$_{0.5}$Mn$_{1.5}$O$_4$ high-voltage spinel for lithium-ion batteries. J. Phys. Chem. C *117*, 15947–15957.

31. Geng, Z., Lu, J., Li, Q., Qiu, J., Wang, Y., Peng, J., Huang, J., Li, W., Yu, X., and Li, H. (2019). Lithium metal batteries capable of stable operation at elevated temperature. Energy Storage Mater. *23*, 646–652.

32. Lee, K.K., Park, K., Lee, H., Noh, Y., Kossowska, D., Kwak, K., and Cho, M. (2017). Ultrafast fluxional exchange dynamics in electrolyte solvation sheath of lithium-ion battery. Nat. Commun. *8*, 14658.

33. Daniel, L., Enea, S.F., Heinz, M.V., Patrik, S., and Corsin, B. (2022). Elucidating the rate-limiting processes in high-temperature sodium-metal chloride batterie. Adv. Sci. *9*, e2201019.

34. Dong, N., Yang, G., Luo, H., Xu, H., Xia, Y., and Liu, Z. (2018). A LiPO$_2$F$_2$/LiFSI dual-salt electrolyte enabled stable cycling of lithium metal batteries. J. Power Sources *400*, 449–456.

35. Fulfer, K.D., and Kuroda, D.G. (2018). Ion speciation of lithium hexafluorophosphate in dimethyl carbonate solutions: an infrared spectroscopy study. Chem. Phys. *20*, 22710–22718.

36. Martinez, A.C., Rigaud, S., Grugeon, S., Tran-Van, P., Armand, M., Cailleu, D., Pilard, S., and Laruelle, S. (2022). Chemical reactivity of lithium difluorophosphate as electrolyte additive in LiNi$_{0.6}$Co$_{0.2}$Mn$_{0.2}$O$_2$/graphite cells. Electrochim. Acta *426*, 140765.

37. Liu, X., Shen, X., Li, H., Li, P., Luo, L., Fan, H., Feng, X., Chen, W., Ai, X., Yang, H., and Cao, Y. (2021). Ethylene carbonate-free propylene carbonate-based electrolytes with excellent electrochemical compatibility for Li-ion batteries through engineering electrolyte solvation structure. Adv. Energy Mater. *11*, 2003905.

38. Cheng, F., Zhang, X., Wei, P., Sun, S., Xu, Y., Li, Q., Fang, C., Han, J., and Huang, Y. (2022). Tailoring electrolyte enables high-voltage Ni-rich ncm cathode against aggressive cathode chemistries for Li-ion batteries. Sci. Bull. *67*, 2225–2234.

39. Mao, M., Huang, B., Li, Q., Wang, C., He, Y.B., and Kang, F. (2020). In-situ construction of hierarchical cathode electrolyte interphase for high performance LiNi$_{0.8}$Co$_{0.1}$Mn$_{0.1}$O$_2$/Li metal battery. Nano Energy *78*, 105282.

40. Mu, L., Lin, R., Xu, R., Han, L., Xia, S., Sokaras, D., Steiner, J.D., Weng, T.C., Nordlund, D., Doeff, M.M., et al. (2018). Oxygen release induced chemomechanical breakdown of layered cathode materials. Nano Lett. *18*, 3241–3249.

41. Liu, L., Gu, S., Wang, S., Zhang, X., and Chen, S. (2020). A LiPO$_2$F$_2$/LiPF$_6$ dual-salt electrolyte enabled stable cycling performance of nickel-rich lithium-ion batteries. RSC Adv. *10*, 1704–1710.

42. Kumar, P., Bharadwaj, M.D., and Yashonath, S. (2016). Effect of interionic interactions on the structure and dynamics of ionic solvation shells in aqueous electrolyte solutions. RSC Adv. *6*, 114666–114675.

STAR★METHODS

KEY RESOURCES TABLE

REAGENT or RESOURCE	SOURCE	IDENTIFIER
Chemicals, peptides, and recombinant proteins		
lithium hexafluorophosphate salt (water content <10 ppm)	Guangdong Candlelight New Energy Technology Co., Ltd	CAS#:1312-81-8
dimethyl carbonate solvent (water content <100 ppm)	Guangdong Candlelight New Energy Technology Co., Ltd	CAS#:616-38-6
$LiNi_{0.5}Mn_{1.5}O_4$	Shenzhen Baxter New Energy Materials Co., Ltd.	MA-EN-CA-29015Y
Acetylene black	Shenzhen Baxter New Energy Materials Co., Ltd.	MA-EN-CO-040161
Polyvinylidene fluoride	Alfa Aesar	CAS#:24937-79-9
N-methyl-2-pyrrolidone	Alfa Aesar	CAS#:120-94-5
Critical commercial assays		
Linear sweep voltammetry	LAND-CT2001A tester	DH7000
Cyclic voltammetry	LAND-CT2001A tester	DH7000
Scanning electron microscopy	Germany ZEISS	Sigma 300
X-ray Photoelectron Spectroscopy	America Thermo Scientific	ESCALAB 250Xi
Fourier Transform Infrared Spectroscopy	America Nicolet	Nicolet 6700
Energy Dispersive Spectrometer	Germany ZEISS	JSM-6100
Inductively Coupled Plasma Optical Emission Spectrometer	America Thermo Scientific	Aglient 5110
NMR spectrometer	BRUKER	VANCEIIIHD500
Deposited data		
Structure of compound	This paper	GaussView 6.0
Software and algorithms		
Gaussian16	Frish et al.	https://gaussian.com

RESOURCE AVAILABILITY

Lead contact

Further information and requests for resources and reagents should be directed to and will be fulfilled by the lead contact, Shiyou Li (lishiyoulw@163.com).

Materials availability

All data are available in the manuscript text. This study did not generate new unique reagents, all the reagents used in this work are commercially available.

Data and code availability

● Structure data used for the simulation included $LiF-PF_6^-$, $LiF-PO_2F_2^-$, $LiPO_2F_2$, CH_3CO_3Li, and HF are deposited, DOi is in the key resources table.

● All original code has been deposited at Zenodo and is publicly available as of the date of publication. DOIs are listed in the key resources table.

● Any additional information required to reanalyze the data reported in this paper is available from the lead contact upon request.

METHOD DETAILS

Preparation of electrolytes and electrodes

The lithium hexafluorophosphate salt [$LiPF_6$ (water content <10 ppm)] and dimethyl carbonate solvent [DMC (water content <100 ppm)] were all purchased from Guangdong Candlelight New Energy Technology Co., Ltd. Electrolytes of $LiPF_6$ in DMC with different salt concentrations were prepared by dissolving

0.7596 g or 4.1775 g of LiPF$_6$ salt in 5 mL DMC solvent and sonicating to prepare solutions of CCEs and HCEs. The salt-to-solvent molar ratios ranged from 1:1 to 5.5:1 and were denoted as 1 M LiPF$_6$/DMC or 5.5 M LiPF$_6$/DMC, respectively. The preparation was conducted in an argon glovebox with water and oxygen content below 0.1 ppm. The ionic conductivity and the viscosities of 1 M LiPF$_6$/DMC and 5.5 M LiPF$_6$/DMC are 3.97 mS cm-1, 1.69 mm^2 s^{-1} and 3.80 mS cm^{-1}, 54.45 mm^2 s^{-1}, respectively. Those electrodes were fabricated by mixing the active materials of LiNi$_{0.5}$Mn$_{1.5}$O$_4$ (LNMO) (from Shenzhen Baxter New Energy Materials Co., Ltd.), acetylene black (Shenzhen Baxter New Energy Materials Co., Ltd.), and polyvinylidene fluoride (Alfa Aesar) binder with a mass ratio of 8:1:1 in N-methyl-2-pyrrolidone (NMP, Alfa Aesar). The resultant slurry was coated evenly on aluminum foil by a film applicator (150 μm thickness) and then dried under vacuum at 110°C for 12 h, which loading amount was around 1.2–2.0 mg cm^{-2} after drying.

Battery assembly and electrochemical measurements

The CR2025 type LNMO||Li half cell with the prepared LNMO cathode, a lithium foil as the anode, a Celgard 2400 film as the spacer, and about 40 μL electrolyte (1 M LiPF$_6$/DMC or 5.5 M LiPF$_6$/DMC), were assembled in a glove box. All electrochemical performances were performed on the LAND-CT2001A tester (Wuhan, China), and the voltage range was from 3.5 to 5.0 V at 2C, 55°C. Linear sweep voltammetry (LSV), chronoamperometry, and cyclic voltammetry (CV) tests were performed on the DH7000 (Jiangsu Dong Hua, China). The CV curves were tested at the potential range of 3.5–5.0 V with a scanning rate from 0.1 to 1.0 mV s^{-1} at 55°C. The chronoamperometry was completed at Li||Al half cells under 5.0 V after preserving three days at 55°C.

Characterization

The scanning electron microscopy (SEM, JSM5600) was used to characterize aluminum foil corrosion and the morphology of LNMO cathode in the LNMO||Li half cells after 200 cycles at 2C, 55°C. X-ray Photoelectron Spectroscopy (XPS, Axis Ultra DLD, Kratos Analytical Ltd.) and Fourier Transform Infrared Spectroscopy (FTIR, America Nicolet) were used to analyze the decomposition products of the two electrolytes on the LNMO surface and dissolution in the electrolyte. FTIR spectra were collected in the range from 2400 to 600 cm^{-1}. The content of transition metals deposited on the LNMO cathode surface or separator added with 0.1% Ferrocene solution as Internal Standard was tested by Energy Dispersive Spectrometer (EDS, JSM-6100) and Inductively Coupled Plasma Optical Emission Spectrometer (ICP-OES, Aglient 5110).

Theoretical calculations

All calculations are performed using the Gaussian 16 package by the DFT method. The geometry optimization and the binding energy calculation were conducted with the basis set of B3LYP/6-311 + G (2 d, p) to analyze the weak interaction between LiF and PF$_6^-$ or PO$_2$F$_2^-$. In addition, the relative Gibbs free energy was calculated at 298.15 K to analyze the reactivity of the LiPO$_2$F$_2$ and CH$_3$CO$_3$Li with the HF molecule.